

11-1-2022

Robust cryogenic ab-initio quantum transport simulation for $L_G = 10$ nm nanowire

Tom Jiao
San Jose State University

Hiu Yung Wong
San Jose State University, hiuyung.wong@sjsu.edu

Follow this and additional works at: https://scholarworks.sjsu.edu/faculty_rsca

Recommended Citation

Tom Jiao and Hiu Yung Wong. "Robust cryogenic ab-initio quantum transport simulation for $L_G = 10$ nm nanowire" *Solid-State Electronics* (2022). <https://doi.org/10.1016/j.sse.2022.108440>

This Conference Proceeding is brought to you for free and open access by SJSU ScholarWorks. It has been accepted for inclusion in Faculty Research, Scholarly, and Creative Activity by an authorized administrator of SJSU ScholarWorks. For more information, please contact scholarworks@sjsu.edu.



Robust cryogenic *ab-initio* quantum transport simulation for $L_G = 10$ nm nanowire

Tom Jiao, Hiu Yung Wong*

Electrical Engineering, San Jose State University, CA, USA

ARTICLE INFO

The review of this paper was arranged by Francisco Gamiz

Keywords:

Ab initio
Cryogenic electronics
Nanowire
Quantum transport
Subthreshold slope

ABSTRACT

In this paper, we propose a simulation methodology for robust and accurate *ab-initio* quantum transport simulation down to 3 K of an *n*-type Si nanowire. This is important to understand the subthreshold swing (SS) at cryogenic temperature. We show that for $L_G = 10$ nm, the SS is fully dominated by direct tunneling at cryogenic temperature, which is the first time to be demonstrated using *ab-initio* simulation, to the best of our knowledge. We propose a method to achieve more than 2x speed up in the simulation time and achieve convergence at high gate biases. It is also shown that from the leakage perspective, there is no advantage in operating $L_G = 10$ nm transistor below 77 K.

1. Introduction

Cryogenic electronics is important for many mission-critical applications such as quantum computer and quantum sensing interfaces [1], space exploration electronics [2], and high-performance cryogenic servers [3]. Technology Computer-Aided Design (TCAD) offers a very cost-effective way of exploring the design space of cryogenic electronics and there has been tremendous progress in the calibration, modeling, and simulation methodologies of cryogenic electronic simulation recently [4–7]. However, cryogenic *ab-initio* quantum transport simulation, which is important to study devices with $L_G < 20$ nm and, particularly, *their sub-threshold behavior, is still difficult and not studied systematically*. It is known that the SS of MOSFET does not follow the Boltzmann statistics [4–9]. To understand its origin, a robust *ab initio* transport simulation setup is needed. To the best of our knowledge, there is no *ab-initio* simulation of cryogenic transport in the literature yet. Only research using Non-Equilibrium Green's Function (NEGF) has been conducted [10].

In this paper, we successfully used *ab-initio* simulation to study the transport characteristics of an $L_G = 10$ nm nanowire at a temperature down to 3 K. The simulation know-how is studied for faster and more robust simulations. The nanowire's cryogenic leakage characteristics are then investigated.

2. Simulation structure and setup

QuantumATK is used in this study [11]. The material used in this paper is Silicon cleaved in the $\langle 100 \rangle$ direction. It is then repeated twice along the transverse directions (A and B), and passivated with hydrogen using sp^3 hybridization. The structure is relaxed using LCAO with GGA for exchange–correlation and PseudoDojo for pseudopotential. The cutoff density is increased to 80 Hartree for better convergence. The force tolerance for the relaxation process is set to 0.01 eV/Å for better accuracy.

The relaxed structure is then repeated 60 times such that it is 32.5 nm in the transport direction, and a cylindrical gate of L_G is added (Fig. 1). Vacuum is formed between the gate and the silicon nanowire which results in an equivalent oxide thickness (EOT) of about 1.6 nm. An electrode length of 5.4 nm is used for both the source and drain electrodes. The same LCAO settings are used for quantum transport simulation. Since it is a gate-all-around (GAA) structure, the Dirichlet boundary condition is applied in all directions in the Poisson solver. To achieve a reasonable simulation time, the parallel conjugate gradient is used for the Poisson solver.

The *n*-type Source/Drain is doped to a level such that the Fermi level is above the conduction band using the compensation charge method. The channel is doped with p-type. It is important to note that the doping should only be applied to the Silicon atoms and not the Hydrogen atoms.

* Corresponding author.

E-mail address: hiuyung.wong@sjsu.edu (H.Y. Wong).

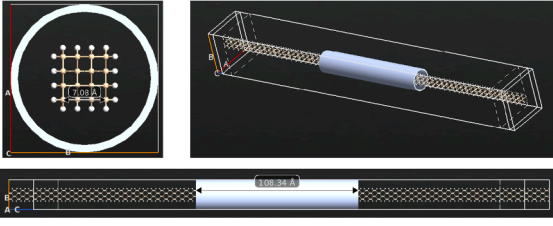


Fig. 1. The cross-section and 3D views of the nanowire simulated. $L_G = 10$ nm is shown. Gate radius is 9 \AA . Gate dielectric is vacuum with $\epsilon_{OT} \sim 1.6$ nm.

3. Energy broadening

The typical *ab-initio* calculation uses the electron ground state energy for calculations and, thus, the quantities calculated such as the transmission coefficient and Local Density of States (LDOS) are for 0 K . However, the convergence can be very bad due to the step-like discontinuity in electron occupation at 0 K (abruptly changes from one below the Fermi level to zero above the Fermi level). This is a common problem in metals as the Fermi Level is within the band. However, the same issue occurs for heavily doped source and drain in Silicon (which is required in cryogenic simulations and will be discussed later). Often, energy broadening is applied to the Fermi-Dirac (FD) distribution in the calculation to smear out the electron distribution for better convergence. This means that the occupation numbers, zero and one, are replaced by a fractional occupation given by FD distribution [12]. Note that this is *not* the FD distribution at the electrodes. Eq. (1) shows the FD distribution equation with T_B being the broadening temperature and kT_B representing the energy broadening. The occupation probability of a state at energy ϵ is,

$$f = \left(1 + e^{\frac{\epsilon - \mu}{kT_B}}\right)^{-1} \quad (1)$$

where k and μ are the Boltzmann constant and Fermi energy, respectively.

At room temperature simulations, sometimes T_B as large as 1000 K is used for good convergence [12]. Fig. 2 shows the $I_D V_G$ simulated with various T_B and electrode temperatures, T , for an $L_G = 5$ nm nanowire. Note that T represents the operating temperatures of the device as it determines the electron distribution at the electrodes, and T_B is just the parameter for electron structure calculations. For $T = 300 \text{ K}$, consistent results are obtained with $T_B < 200 \text{ K}$. However, $T_B < 5 \text{ K}$ is required for $T = 3 \text{ K}$ simulation. Therefore, $T_B = 5 \text{ K}$ is used in this study.

While setting $T_B = 5 \text{ K}$ might make the convergence more difficult, it brings another positive effect toward more accurate and robust simulations. It is found that a large T_B can cause Fermi level in the heavily doped source/drain to shift into the bandgap. Fig. 3 shows that when the doping is 10^{21} cm^{-3} and $T_B = 1000 \text{ K}$, the Fermi level is below the CB by 80 meV and there is finite current for $T = 300 \text{ K}$ but almost no current for $T = 10 \text{ K}$ or below. However, using large S/D doping will worsen the

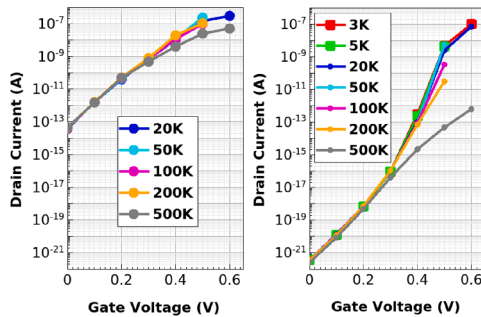


Fig. 2. $I_D V_G$ of the nanowire with $L_G = 5$ nm at $T = 300 \text{ K}$ (Left) and $T = 3 \text{ K}$ (Right) with various T_B . $V_D = 50 \text{ mV}$.

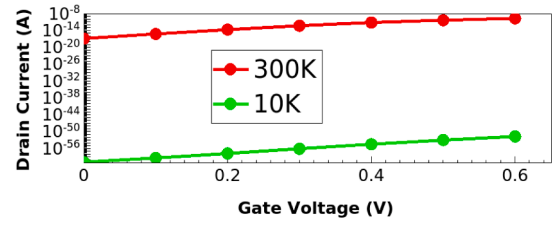


Fig. 3. $I_D V_G$ of the nanowire with $L_G = 5$ nm at $T = 300 \text{ K}$ and $T = 10 \text{ K}$ when the Fermi level is 80 meV below the CB with S/D doping of 10^{21} cm^{-3} and $T_B = 1000 \text{ K}$. $V_D = 50 \text{ mV}$.

convergence due to the large doping gradient between the S/D and the channel.

Fortunately, smaller T_B provides more accurate simulation and smaller S/D doping is required to keep the Fermi level above the conduction band at the same time. Fig. 4 shows the S/D doping concentration required to keep the Fermi level around 18 meV above the CB at various T_B . This is critical in cryogenic applications such as quantum computing since at these temperatures, thermionic emission and thus transport, is almost impossible when the Fermi energy in the source region is below the conduction band edge. With $T_B = 5 \text{ K}$, only $5 \times 10^{20} \text{ cm}^{-3}$ of doping is required. Fig. 5 shows the LDOS of the device studied with the gate and the drain at zero bias and the electrodes' Fermi levels of the optimal setup.

4. Transmission spectrum

The total current in transport calculations is found using Eq. (2), where $T(E, \mu_L, \mu_R)$ is the transmission coefficient found for the structure at a given gate and drain bias, and f is the Fermi distribution function for the left and right electrodes.

$$I = \frac{2q}{h} \int T(E, \mu_L, \mu_R) \left[f\left(\frac{E - \mu_L}{k_B T}\right) - f\left(\frac{E - \mu_R}{k_B T}\right) \right] dE \quad (2)$$

where q , h , μ_L , μ_R , and E are the elementary charge, Planck's constant, Fermi levels at the left and right electrodes, and the energy of the electrons, respectively. Since it is discretized at different energy levels, the density of the transmission points must not be too low to capture the correct current, especially at low temperatures. For this study, the transmission spectrum covers the range of -1 to 4 eV , with respect to the source's Fermi energy, and this gives a resolution of 10 meV per transmission point.

The transmission spectrum is plotted in Fig. 6 for two gate voltages. Transmission for $V_G = 1 \text{ V}$ is higher than 0.4 V due to the lowering of the gate barrier. However, note that the transmission is not zero for energy levels that are below the barrier (0.04 eV for $V_G = 0.4 \text{ V}$). This tunneling current will degrade the SS as shown in the next section.

5. Nanowire simulation results

The SS slope of an $L_G = 10 \text{ nm}$ GAA nanowire is then studied at

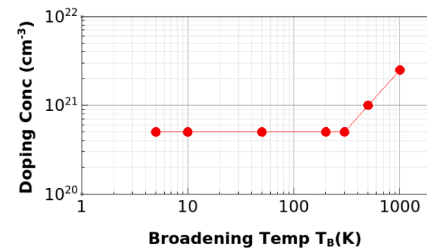


Fig. 4. Source/Drain doping concentration required to keep the Fermi level 18 meV above the CB.

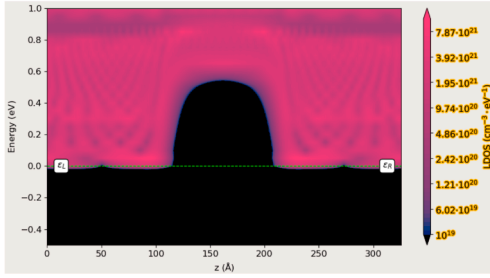


Fig. 5. LDOS of the nanowire with $V_G = 0$ V. $T_B = 5$ K is used. $L_G = 10$ nm. S/D doping is 5×10^{20} cm^{-3} .

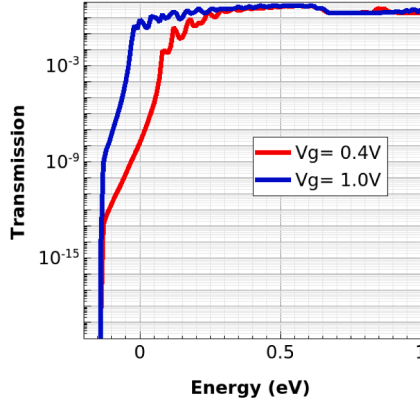


Fig. 6. Transmission spectrum of an $L_G = 10$ nm nanowire at $V_G = 0.4$ V and $V_G = 1$ V. Both with $V_D = 50$ mV.

various electrode/operation temperatures, T , using $T_B = 5$ K and S/D doping of 5×10^{20} cm^{-3} . To further improve convergence, $T_B = 300$ K is used as an initial solution at $V_G = 0$ V and $V_D = 50$ mV. And then T_B is reduced gradually to 5 K. Fig. 7 shows the $I_D V_G$ curves. The full IV curve is possible because of the robust setup. Fig. 8 shows the speed up by using lower S/D doping (5×10^{20} cm^{-3}) which is enabled by using $T_B = 5$ K.

From Fig. 7a, it can be seen that the subthreshold slope stops following the Boltzmann statistics ($SS = \ln(10)kT/q$) when $T < 77$ K. It is believed that this is because the tunneling current, which does not follow $\ln(10)kT/q$ as the barrier changes, dominates over the thermionic current, which follows $\ln(10)kT/q$. As shown in Fig. 7b, the spectral current at 3 K are nonzero only in the region below the barrier even at $V_G = 0.55$ V (right before it is turned on).

To further prove that the abnormal subthreshold slope is due to the

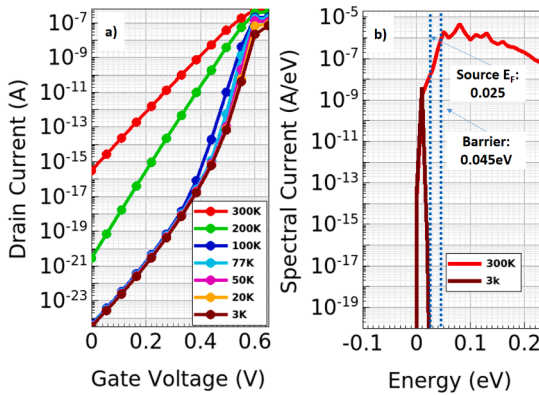


Fig. 7. a) $I_D V_G$ of the nanowire with $L_G = 10$ nm at various T with $T_B = 5$ K and S/D doping of 5×10^{20} cm^{-3} . b) Spectral current at $V_G = 0.55$ V at 300 K and 3 K.

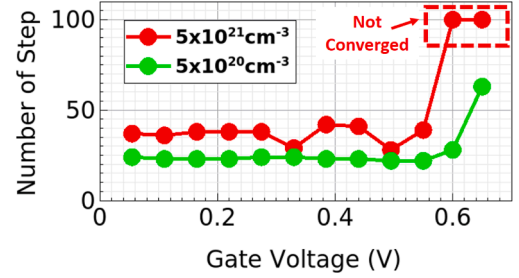


Fig. 8. Number of steps to achieve convergence at each gate bias for the $I_D V_G$ in Fig. 7.

tunneling current, the current as a function of gate voltage is fit against the transmission coefficient as a function of the barrier height calculated with WKB approximation.

In the WKB approximation, a rectangular barrier is used with the width and height measured from the LDOS plots of the corresponding V_G . The band edge of Silicon is typically thought to be at when the density of states in the Conduction Band (CB) and the Valance Band (VB) is at around 3×10^{19} and 1×10^{19} states per cm^3 , respectively. Therefore, this is used for barrier height extraction. It should be noted that since the nanowire is finite in size, unlike an infinitely larger silicon crystal, the band edges cannot be absolutely sharp. That means, there is a non-zero density of states in the bandgap. Fig. 9 shows the LDOS for $V_g = 0.4$ V and the lower cutoff for the LDOS is at 3×10^{19} states per cm^3 to reflect the nominal band edge. The figure also shows the LDOS with a lower cutoff, at 1×10^{18} states per cm^3 . It can be seen that their barrier heights and widths are different. 3×10^{19} states per cm^3 is used in the extraction.

The transmission coefficient from WKB is shown in Eq. (3) with a and V being the barrier height and width, respectively, and m^* is the tunneling electron mass. The actual transmission spectrum, T , is extracted from the simulation.

$$T \propto \exp\left(-2a \frac{\sqrt{2m^*V}}{\hbar}\right) \quad (3)$$

The dependence of the current on V_G is found to fit the equation well in the subthreshold region if the effective electron mass, m^* , is set to $0.35 m_0$. Therefore, the leakage is dominated by the tunneling current.

Finally, since the leakage current does not reduce at 77 K or below, there is no advantage in going to $T = 3$ K operation in terms of off-state leakage unless a very low V_{TH} device is needed as there is still a 10X reduction in leakage at 0.5 V from 77 K to 3 K (equivalent to having $V_{TH} = 0.1$ V).

6. Conclusions

For the first time, we completed a full $I_D V_G$ simulation of an $L_G = 10$ nm nanowire at $T = 3$ K. We proposed a methodology to achieve an accurate and robust cryogenic *ab initio* quantum transport simulation

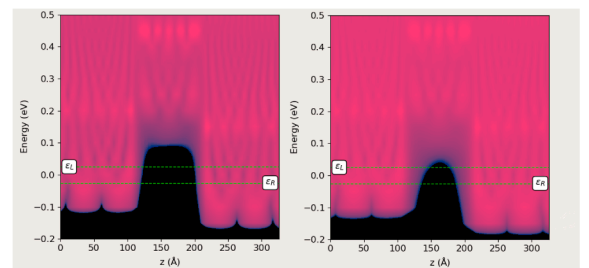


Fig. 9. LDOS plots for $V_g = 0.4$ V, at 3×10^{19} states per cm^3 cutoff (left) and 1×10^{18} states per cm^3 cutoff (right).

down to 3 K. It is proved that the leakage is dominated by tunneling at 3 K but there is about a 10X reduction in leakage if a $V_{TH} = 0.1$ V device is used.

Declaration of Competing Interest

The authors declare the following financial interests/personal relationships which may be considered as potential competing interests: Hiu Yung Wong reports financial support was provided by National Science Foundation.

Data availability

Data will be made available on reasonable request.

Acknowledgments

This material is based upon work supported by the National Science Foundation under Grant No. 2046220. The authors thank Dr. Anders Blom from QuantumATK, Synopsys Inc. for his support and discussion.

References

- [1] Charbon, et al. Cryo-CMOS for Quantum Computing. 2016 IEEE international electron devices meeting (IEDM), San Francisco, CA. 2016. pp. 13.5.1-13.5.4.
- [2] Gong MJ, et al. Design considerations for spin readout amplifiers in monolithically integrated semiconductor quantum processors. In: 2019 IEEE radio frequency integrated circuits symposium (RFIC), Boston, MA, USA; 2019. p. 111–4.
- [3] Patterson RL, et al. Electronics for deep space cryogenic applications. In: Proceedings of the 5th European Workshop on Low Temperature Electronics, Grenoble, France; 2002. p. 207–10.
- [4] Beckers A. Cryogenic MOSFET modeling for large-scale quantum computing. Ph.D. dissertation. Faculté des sciences et techniques de l'ingénieur, Lausanne, EPFL; 2021.
- [5] Wong HY. Calibrated Si Mobility and Incomplete Ionization Models with Field Dependent Ionization Energy for Cryogenic Simulations. In: 2020 international conference on simulation of semiconductor processes and devices (SISPAD), Kobe, Japan; 2020. p. 193–6.
- [6] Dhillon P, Wong HY. A wide temperature range unified undoped bulk silicon electron and hole mobility model. IEEE Trans Electron Devices April 2022;69(4): 1979–83. <https://doi.org/10.1109/TED.2022.3152471>.
- [7] Dhillon P, Dao NC, Leong PHW, Wong HY. TCAD modeling of cryogenic nMOSFET ON-state current and subthreshold slope. In: 2021 International conference on simulation of semiconductor processes and devices (SISPAD); 2021. p. 255–8. <https://doi.org/10.1109/SISPAD54002.2021.9592586>.
- [8] Hafez IM, Ghibaudo G, Balestra F. Assessment of interface state density in silicon metal-oxide-semiconductor transistors at room, liquid-nitrogen, and liquid-helium temperatures. J Appl Phys 1990;64(4):1950–2. <https://doi.org/10.1063/1.345572>.
- [9] Bohuslavskiy H, Jansen AG, Barraud S, Barral V, Casse M, Le Guevel L, et al. Cryogenic subthreshold swing saturation in FD-soi mosfets described with band broadening. IEEE Electron Device Lett 2019;40(5):784–7.
- [10] Kao K-H, Wu TR, Chen H-L, Lee W-J, Chen N-Y, Ma W-Y, et al. Subthreshold swing saturation of nanoscale MOSFETs due to source-to-drain tunneling at cryogenic temperatures. IEEE Electron Device Lett 2020;41(9):1296–9.
- [11] Søren Smidstrup et al., “QuantumATK: an integrated platform of electronic and atomic-scale modelling tools,” J. Phys.: Condens. Matter 32 (2020) 015901 (36pp).
- [12] QuantumATK™ Reference Manual Version S-2021.06, June 2021.